SYNTHESIS OF NANOSTRUCTURED METAL OXIDES FOR GAS SENSORS

M.Kh.Kuchkarov
Associate Professor of the Department of Physics and Astronomy

Abstract. Semiconducting metal oxides are the dominant transduction materials for chemiresistive gas sensors, and their performance is governed by the surface-to-volume ratio, crystallite size and morphology that nanostructuring makes accessible. This work reviews the principal vapour- and solution-phase routes used to synthesise nanostructured metal oxides for gas sensing—sol–gel processing, spray pyrolysis, chemical and physical vapour deposition, template filling, and hydro-/solvothermal growth—and links each architecture to the underlying sensing physics. Representative systems include template-grown SnO_2 nanotubes, carbothermal one-dimensional In_2O_3 and Ga_2O_3, hydrothermal porous α-Fe_2O_3, ultrathin p-type CuO nanoribbons, and Co_3O_4 hollow nanospheres. A compact mathematical framework—the Debye-length depletion model, the double-Schottky-barrier grain-size effect, and the Knudsen diffusion–reaction equation—rationalises the measured responses, which are maximised when the feature size approaches twice the depletion-layer thickness and gas access to interior sites is preserved by controlled porosity.

Keywords: *metal oxide; gas sensor; nanostructure; chemiresistive sensing; hydrothermal synthesis; grain-size effect.*

1. Introduction

Gas sensors warn against flammable and toxic species and thereby protect lives and property; their value is set by two figures of merit, sensitivity and selectivity [4]. Among device families, chemiresistive sensors based on semiconducting metal oxides—pioneered by the Taguchi-type SnO_2 element—remain the most widely deployed because they are inexpensive, robust and simple to read out [1]. Their conductance changes reversibly when chemisorbed oxygen reacts with the target gas, a modulation confined to a near-surface depletion layer and therefore dictated by microstructure. Nanostructuring increases the active surface area and brings characteristic feature sizes down to the depletion-layer scale, which is the principal lever for improving response. This paper surveys the main synthesis routes, develops the governing mathematical framework, and connects both to a set of representative oxides studied in a recent doctoral investigation [1].

2. Synthesis of nanostructured metal oxides

Synthesis methods fall into two families. Vapour-phase routes—chemical and physical vapour deposition (CVD/PVD), spray pyrolysis and carbothermal evaporation following vapour–liquid (VL) or vapour–liquid–solid (VLS) growth—yield highly crystalline one-dimensional (1D) nanowires and nanobelts with well-defined facets [1,7]. Solution-phase routes—sol–gel processing, template filling, and hydro-/solvothermal growth—give porous and hollow architectures with tunable grain size and pore structure [8].

In template filling, a precursor infiltrates a sacrificial template to form SnO_2 nanotubes whose walls can be made thinner than twice the depletion width, maximising the fraction of fully depleted material [1]. Carbothermal CVD produces 1D In_2O_3 and Ga_2O_3 nanowires whose crystallinity exposes defined facets, although large wire diameters limit the active surface. Hydrothermal growth gives porous α-Fe_2O_3 nanorods, nanowires or nanospheres by tuning source material, temperature and reaction time, providing direct geometric control [1]. Surfactant-assisted solvothermal synthesis yields Co_3O_4 hollow nanospheres of 200–300 nm with high catalytic activity [6], and decorating CuO nanoribbons with Au or Pt adds catalytic sensitisation. Table 1 summarises the systems considered here.

Table 1. Representative nanostructured metal oxides, synthesis routes, morphologies and target gases [1,6].

Material	Synthesis route	Morphology	Target gas
SnO_2 (n)	Template filling	Nanotubes	H_2, CO, C_2H_5OH
In_2O_3, Ga_2O_3 (n)	Carbothermal CVD (VLS)	Nanowires (1D)	C_2H_5OH, NO_2
α-Fe_2O_3 (n)	Hydrothermal	Porous rods / wires / spheres	C_2H_5OH, acetone
CuO (p)	Solution + Au/Pt loading	Nanoribbons, 2–8 nm	H_2S, CO
Co_3O_4 (p)	Surfactant solvothermal	Hollow nanospheres	Toluene, acetone

3. Sensing mechanism and mathematical apparatus

Receptor function. Atmospheric oxygen adsorbs on the oxide surface and ionosorbs by capturing conduction electrons, following

$$O_2(gas) + \beta e^- \rightarrow O_2^{\beta-}(ads) \quad (1)$$

where β = 1 or 2 selects the ionic species (O^- or O^{2-}). Electron trapping depletes the near-surface region and bends the energy bands upward, raising the resistance. On exposure to a reducing gas such as CO, the surface oxidation

$$CO(gas) + O^-(ads) \rightarrow CO_2(gas) + e^- \quad (2)$$

Transducer function. returns electrons to the conduction band and lowers the resistance of an n-type oxide. In polycrystalline films, inter-grain transport is controlled by double Schottky barriers [5]; the depletion-layer thickness is

$$L_s = L_D\sqrt{\frac{eV_s}{kT}} \quad (3)$$

with the Debye length

$$L_D = \sqrt{\frac{\varepsilon kT}{2\pi e^2 N_d}} \quad (4)$$

where k is the Boltzmann constant, T the temperature, V_s the Schottky potential, e the elementary charge, ε the permittivity and N_d the donor density.[1] The response therefore depends on the ratio of crystallite size D to $2L_s$. Three regimes follow (Fig. 1a): boundary-controlled ($D \gg 2L_s$), neck-controlled, and grain-controlled ($D \leq 2L_s$), where the response rises steeply because grains become almost fully depleted [2].

Geometric (diffusion) function. The target gas must diffuse to interior sites while it is consumed by reaction. Assuming Knudsen diffusion[2] and first-order kinetics, the concentration C_A obeys

$$D_K\frac{\partial^2 C_A}{\partial x^2} - kC_A = \frac{\partial C_A}{\partial t} \quad (5)$$

whose steady-state solution ($\partial C_A/\partial t = 0$) for a film of thickness L is

$$C_A = C_{A,s}\frac{\cosh(L-x)\sqrt{\frac{k}{D_K}}}{\cosh L\sqrt{\frac{k}{D_K}}} \quad (6)$$

Equation (6) is plotted in Fig. 1b: when $\sqrt{(k/D_K)} \gtrsim 10^{-2}$ nm^{-1} the gas is consumed near the surface and the interior is unused, whereas low values give a flat profile and full utilisation [3]. The sensitivity of an n-type sensor to a reducing gas is defined by the resistance ratio,

$$S = \frac{R_{air}}{R_{gas}} \quad (7)$$

Empirically the response follows a power law in concentration, $S = a\cdot C_{gas}^{\beta}$, with exponent $\beta \approx 0.5$–1 set by the dominant oxygen species [3,4]. The dynamic transient (Fig. 2) defines the response time t_{res} (90 % of the resistance change) and the recovery time t_{rec} (return to within 10 % of baseline).

---

[1]Gaussian-unit form, where ε is the static permittivity and N_e the donor (carrier) density; L_e typically spans 1–100 nm for SnO_2 [2].

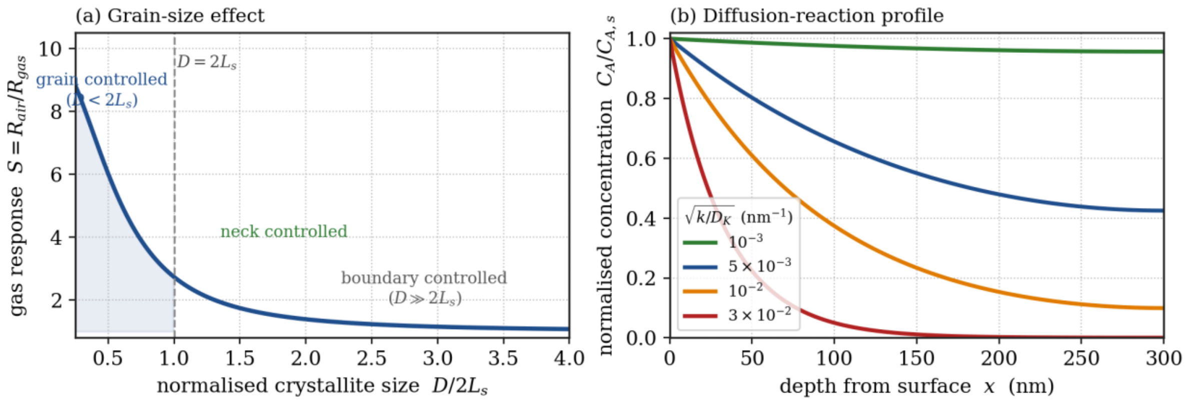

Pic. 1. (a) Gas response $S = R_{air}/R_{gas}$ as a function of normalised crystallite size $D/2L_s$, showing the boundary-, neck- and grain-controlled regimes [2]. (b) Normalised target-gas concentration $C_A/C_{A,s}$ versus depth x inside a 300 nm film from Eq. (6), for several values of $\sqrt{(k/D_K)}$ [3].

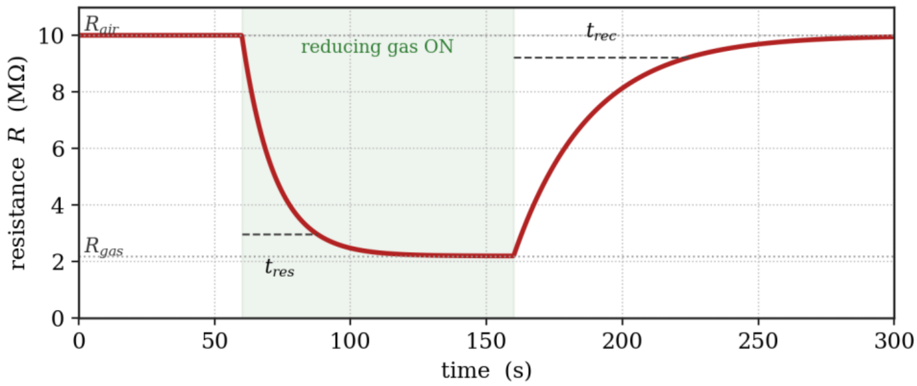

Pic. 2. Simulated chemiresistive transient of an n-type oxide on exposure to a reducing-gas pulse, defining the response time t_{res} and recovery time t_{rec} between the air baseline R_{air} and the in-gas value R_{gas}.

4. Results and discussion

Mapping morphology onto Eqs. (3)-(6) explains the measured trends. SnO_2 nanotubes outperform nanoparticles because their thin walls lie within the depletion scale, so a larger material fraction responds [1]. The 1D In_2O_3 nanowires show only moderate response and Ga_2O_3 is essentially inactive: their lateral dimensions greatly exceed $2L_s$, so the depleted shell is a small fraction of the wire and the crystallographic-plane advantage cannot be exploited unless the wires are thinned [1]. In porous α-Fe_2O_3 the architecture differentiates the signal below 200 ppm, consistent with Fig. 1b [1]. Ultrathin p-type CuO nanoribbons (2–8 nm) give unexpectedly high responses, further enhanced by Au/Pt sensitisation, and Co_3O_4 hollow nanospheres expose thin shells modulated through their whole volume, enabling good toluene and acetone detection [6]. Response is thus maximised when the feature size approaches $2L_s$ and open porosity preserves gas access—both predicted by the framework above.

5. Conclusions

Nanostructuring is the principal lever for chemiresistive gas-sensor performance: the synthesis route selects the morphology, and the morphology fixes the balance between surface depletion and diffusion–reaction that the equations above quantify. Designing feature sizes near $2L_s$, maintaining open porosity, and adding noble-metal functionalisation together yield the largest and most selective responses, while faceted 1D crystals require lateral thinning before they become sensor-relevant.

References

[1] J. Park, Nanostructured semiconducting metal oxides for use in gas sensors, Ph.D. thesis, University of Wollongong, Wollongong, 2010.

[2] C. Xu, J. Tamaki, N. Miura, N. Yamazoe, Grain size effects on gas sensitivity of porous SnO_2-based elements, Sens. Actuators B 3 (1991) 147–155.

[3] G. Sakai, N. Matsunaga, K. Shimanoe, N. Yamazoe, Theory of gas-diffusion controlled sensitivity for thin film semiconductor gas sensor, Sens. Actuators B 80 (2001) 125–131.

[4] N. Yamazoe, Toward innovations of gas sensor technology, Sens. Actuators B 108 (2005) 2–14.

[5] N. Bârsan, U. Weimar, Conduction model of metal oxide gas sensors, J. Electroceram. 7 (2001) 143–167.

[6] J. Park, X.P. Shen, G.X. Wang, Solvothermal synthesis and gas-sensing performance of Co_3O_4 hollow nanospheres, Sens. Actuators B 136 (2009) 494–498.

[7] E. Comini, G. Faglia, G. Sberveglieri, Z. Pan, Z.L. Wang, Stable and highly sensitive gas sensors based on semiconducting oxide nanobelts, Appl. Phys. Lett. 81 (2002) 1869–1871.

[8] J.-H. Lee, Gas sensors using hierarchical and hollow oxide nanostructures: Overview, Sens. Actuators B 140 (2009) 319–336.